Photochemistry and Photobiology, 2013, 89: 698–708

Localized *In Vivo* Activation of a Photoactivatable Doxorubicin Prodrug in Deep Tumor Tissue

Stuart Ibsen*[1], Eran Zahavy[2], Wolf Wrasidlo[3], Tomoko Hayashi[3], John Norton[3], Yongxuan Su[4], Stephen Adams[5] and Sadik Esener[6]

[1]Department of Bioengineering, Moores Cancer Center, University of California San Diego, La Jolla, CA
[2]Department of Infectious Disease, Israel Institute for Biological Research, Ness-Ziona, Israel
[3]Moores Cancer Center, University of California at San Diego, La Jolla, CA
[4]Department of Chemistry and Biochemistry, University of California at San Diego, La Jolla, CA
[5]Department of Pharmacology, University of California at San Diego, La Jolla, CA
[6]Department of Nanoengineering, University of California at San Diego, La Jolla, CA

Received 3 October 2012, accepted 5 January 2013, DOI: 10.1111/php.12045

ABSTRACT

Sparing sensitive healthy tissue from chemotherapy exposure is a critical challenge in the treatment of cancer. The work described here demonstrates the localized *in vivo* photoactivation of a new chemotherapy prodrug of doxorubicin (DOX). The DOX prodrug (DOX-PCB) was 200 times less toxic than DOX and was designed to release pure DOX when exposed to 365 nm light. This wavelength was chosen because it had good tissue penetration through a 1 cm diameter tumor, but had very low skin penetration, due to melanin absorption, preventing uncontrolled activation from outside sources. The light was delivered specifically to the tumor tissue using a specialized fiber-optic LED system. Pharmacokinetic studies showed that DOX-PCB had an α circulation half-life of 10 min which was comparable to that of DOX at 20 min. DOX-PCB demonstrated resistance to metabolic cleavage ensuring that exposure to 365 nm light was the main mode of *in vivo* activation. Tissue extractions from tumors exposed to 365 nm light *in vivo* showed the presence of DOX-PCB as well as activated DOX. The exposed tumors had six times more DOX concentration than nearby unexposed control tumors. This *in vivo* proof of concept demonstrates the first preferential activation of a photocleavable prodrug in deep tumor tissue.

INTRODUCTION

Systemically administered chemotherapy is an important treatment option used to reduce tumor mass before surgical removal (1,2) and for primary tumors that have not yet metastasized, such as childhood nonmetastatic Wilms tumor (3). In these cases the chemotherapy needs to be active only in the affected tissue. For the treatment of Wilms tumor, doxorubicin (DOX) or a combination of dactinomycin and vincristine is usually administered before or after the surgical removal of the tumor. The goal is to either shrink the tumor to reduce the possibility of surgical complications, or to kill any tumor margins left behind after the resection (3,4). The 85% positive outcome rate for Wilms tumor treatment makes managing and reducing the chemotherapy-related toxicities the main problem of this disease (3). These toxicities occur because only a small fraction of the injected chemotherapy dose ever reaches the tumor. The excess drug circulates through healthy tissue resulting in detrimental side effects (5). The biggest concerns are adverse effects to the gastrointestinal tract (6) and damage to the hematopoietic system causing suppression of the immune system (6). DOX exposure also increases the chances of long-term cardiomyopathy and congestive heart failure (2,7,8). These side effects are of particular concern in children (9,10).

Reducing the amount of active DOX that reaches the heart and healthy tissue has been shown to reduce these side effects as demonstrated with Doxil®, a liposomal formulation of DOX (11,12). However, major hurdles remain such as the slow release of DOX from the liposomes limiting the maximum levels of bioavailable drug in the tumor over time (13), and nonspecific accumulation of Doxil® in healthy tissue (11,14). Radiofrequency heating (15) and focused ultrasound heating (16) are being evaluated as triggers to cause preferential release of pure DOX from lyso-thermosensitive liposomes specifically in the tumor tissue. However, the liver and other healthy tissues where these vehicles also accumulate will receive a dose of pure DOX once the carriers eventually break down.

Currently there is no reliable way for a clinician to limit the contact of active DOX to a single region within the body. This research focuses on the development of a system where the clinician can use light to highlight a defined region of tissue encompassing the tumor, such as the kidneys for Wilms tumor, creating a zone where a photocleavable DOX prodrug is locally activated to a therapeutic state. The light can be delivered with fiber-optic and light emitting diode (LED) technology. The recent miniaturization of LEDs to as thin as a human hair (17) allows them to be temporarily implanted anywhere a biopsy needle, endoscope or catheter can go. They can also be left in the lesion site after tumor resection. To respond to the delivered light we have developed a prodrug of DOX which uses a covalently bound photocleavable linker (18) to render DOX 200 times less toxic to tissue with the unique ability to restore full therapeutic function when phototriggered (19). The prodrug, referred to as DOX-PCB, was

*Corresponding author email: stuart.ibsen@gmail.com (Stuart Ibsen)

formed by blocking the free amine of the sugar moiety with a nitrophenyl compound conjugated to a short PEG linker and terminated with a biotin (PCB) as shown in Fig. 1. The photocleavable linker was chosen to be resistant to metabolic degradation preventing nonspecific activation of the prodrug in healthy tissue, especially the liver (19,20). This limits activation just to the highlighted tissue region. Systemically administered prodrugs have been shown to substantially lower toxic effects on healthy tissue where they are not activated (8,21,22).

The resistance of DOX-PCB to metabolic activation is different from traditional prodrug designs which have relied heavily on inherent chemical and biochemical properties of the tumor to act as activation triggers. These triggers include environmental differences between the tumor tissue and normal tissue, such as hypoxia or low pH (23,24), enzymatic cleavage by enzymes that are over secreted by the tumor (25–27) and antibody/tumor antigen binding and internalization into the cell where activation is usually triggered by the low pH of the intracellular endosomal environment (28). The challenge is that these triggers often have low contrast between the tumor and healthy tissue (29,30), especially with the normal enzymatic activity of the liver. Tumor cells are also not homogenous in their gene expression (31) and there can be significant differences between tumors from different patients (32) making a standardized trigger difficult to develop. All of these factors make developing a truly tumor-specific biochemical trigger a challenge.

The illumination of the tumor with the custom LED/fiber-optic system provides a stark differentiation between the tumor and the healthy tissue to address these challenges, as the light is found no where else in the body. The light activation trigger is completely independent of the biochemical or environmental properties of the tumor allowing the production of free DOX to be limited to just the highlighted region. The light activation is also independent of the biochemical variability in tumors between patients (33) and can be applied to many different types of solid tumors without requiring prior knowledge of individual tumor biochemistry. The triggering wavelength of 365 nm light was chosen because internal tissue has low absorption of 365 nm light (34), including DNA (35). The 365 nm light is also heavily absorbed by melanin and so does not penetrate significantly more than 1 mm through human skin. This ensures the only significant amount of 365 light present in the body is that delivered to the tumor region. The localized light delivery for the *in vivo* experiments in this work was achieved by using a custom-designed 365 nm LED/fiber-optic system that physically penetrated into the middle of the tumor itself. The high-intensity light could allow for a burst release of DOX inside the tumor tissue allowing the concentration to rise rapidly.

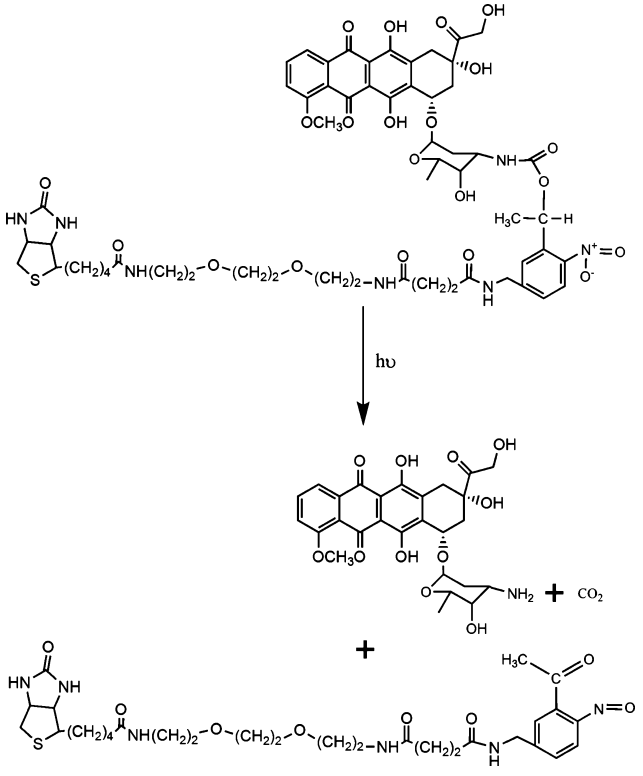

Figure 1. Chemical structure of DOX-PCB with the three products resulting from photocleavage including pure DOX. The molecular weight of DOX-PCB is 1221.44 g mol^{-1}.

This study demonstrates the feasibility of using 365 nm light to activate the DOX-PCB prodrug *in vivo* and cause preferential accumulation of active DOX in the tumor tissue through three sets of experiments.

The first set of experiments quantifies 365 nm light penetration through *ex vivo* tumor tissue and subsequent DOX-PCB activation using the custom-designed 365 nm LED/fiber-optic delivery system.

The second set of experiments look at the circulation half-life and elimination of DOX-PCB in mice to determine the proper time for 365 nm light administration to prevent activation of DOX-PCB in the vasculature.

The third set of experiments look at the *in vivo* activation of DOX-PCB within tumor tissue after systemic administration of DOX-PCB.

MATERIALS AND METHODS

Materials. Doxorubicin hydrochloride (DOX) was obtained from Qventas (Branford, CT) and Sigma (St. Louis, MO). Water soluble photocleavable biotin-NHS (PCB) was purchased from Ambergen (Watertown, MA). The components of the synthesis buffer, $NaCHO_3$ and NaOH, were from EMD (San Diego, CA). High-pressure liquid chromatography (HPLC) grade acetonitrile and methanol were purchased from Fisher Scientific (Fairlawn, NJ). The athymic nu/nu nude mice were purchased from the Jackson Laboratory (Bar Harbor, ME). The human lung cancer cell-line A549 was purchased from the American Type Culture Collection (ATCC) (Manassas, VA). The Captisol® was purchased from Ligand Pharmaceuticals (La Jolla, CA).

Preparation of DOX-PCB. Synthesis of DOX-PCB was preformed as described in Ibsen *et al.* (19). The DOX-PCB was then dissolved in 50 μL of DMSO and was then purified on a semiprep HPLC system using a 10–90 ACN:H_2O 0.05%TFA gradient set over 20 min. The resulting fractions containing the two DOX-PCB isomers were collected and pooled into the same sample. The sample was then lyophilized and stored at −20°C wrapped in foil. A study was conducted that found no difference in biological activity on A549 cells *in vitro* between the two isomeric forms (data not shown) so all the studies presented here have the two isomers pooled together.

365 nm LED/fiber-optic delivery system. A custom designed 365 nm LED/fiber-optic delivery system was developed in collaboration with Prizmatix Ltd. that coupled a fiber optic to a 365 nm LED. The end of the fiber was encased inside a beveled metal tube that was the equivalent of a 22 gauge needle to allow for tumor penetration as shown in Fig. 2.

Tumor preparation. A549 cells were expanded in 25 mL flasks. They were trypsinized and washed with cold PBS. They were then resuspended in cold PBS at a concentration of 1×10^8 cells mL^{-1}. 1.2 mL of the cell suspension was added to 1.2 mL of matrigel and kept on ice.

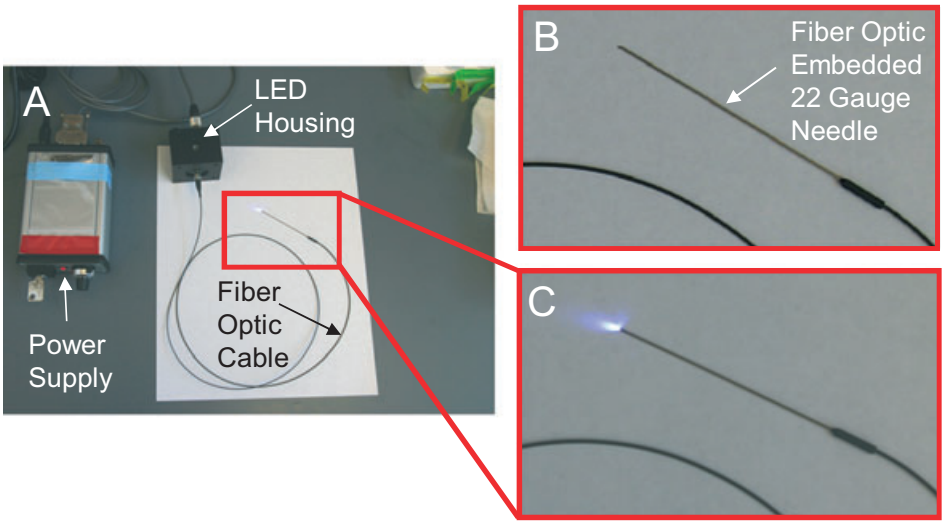

Figure 2. The 365 nm LED/fiber-optic delivery system. (A) The power supply and the LED housing are shown with the fiber-optic cable. As 365 nm light is not directly visible, the end of the cable was placed on a piece of white paper to show the blue autofluorescence of the paper caused by the 365 nm light emitted from the end of the fiber. (B) An expanded view of the fiber-optic embedded in a 22 gauge needle without the 365 nm light. (C) This expanded view shows the 365 nm light coming from the end of the needle causing secondary autofluorescence of the paper which is visible as the blue light.

200 μL of the mixture was injected in the left and right flanks of five female athymic nu/nu nude mice. One of the two tumors in the same mouse would serve as a control and would not receive a 365 nm light dose. The tumors were allowed to grow for 1 month until they reached the size of 1 cm^3. Mice were maintained under standard conditions in the University of California, San Diego Animal Facility. All animal protocols received prior approval by the institutional review board.

Ex vivo 365 nm light penetration of tumor tissue. A Newport 1830-C Optical Power Meter with a Newport 818-UV detector head and a Newport 883-UV OD3 filter was used to measure the intensity of light coming from the 365 nm LED/fiber-optic system turned to max power. Measurements were taken 10 mm directly in front, from the right side and from behind the fiber end. To measure tumor tissue penetration and scattering of the light, the system needle was inserted into the middle of a 9 × 6 × 5 mm tumor prepared in the manner stated above that was collected from a mouse never injected with DOX-PCB or DOX. The measurements were taken again from a distance of 10 mm from the tumor surface.

DOX-PCB activation in ex vivo tumor tissue. An *ex vivo* experiment was run to establish the activatability of DOX-PCB in an actual tumor sample prepared in the manner stated above that was collected from a mouse never injected with DOX-PCB or DOX. The tumor was cut into three sections of 30 mg each. The first sample was injected with 10 μL DMSO containing 224 ng of DOX-PCB and 20 ng of DOX to ensure that a small amount of DOX would be detectable. The other two samples were injected with 10 μL DMSO containing just 224 ng of DOX-PCB. One of these samples was exposed to 30 min of 365 nm light using the LED/fiber-optic system described above. The tissue was allowed to absorb the DMSO for 15 min giving the DMSO enough time to penetrate deep into the sample carrying the dissolved compounds with it. The tissue integrity was not compromised by the DMSO.

DOX-PCB solubilization with Captisol® cyclodextrin. DOX-PCB required a solubilization agent for *in vivo* injection because it displayed low inherent water solubility. DOX-PCB was observed to be soluble in cell culture media if first dissolved in DMSO and injected straight into the media. This apparent solubility was most likely due to DOX-PCB adsorption to proteins found in the media itself because the same injection of DMSO/DOX-PCB into water resulted in instant precipitation. For *in vivo* injection the concentration of DOX-PCB in the injectant needed to be 2 mM which made it necessary to use the well-characterized and nontoxic cyclodextrin solubilizing agent Captisol®. This kept the DOX-PCB soluble in saline at a sufficient concentration without the use of organic solvents to make it safe for injection.

Solubilization of DOX-PCB with the cyclodextrin required the formation of a DOX-PCB solvent complex and possible salt. 1 mg of the lyophilized DOX-PCB powder was dissolved in 500 μL of methanol and dried in a speedvac. The dried DOX-PCB was then dissolved in 50 μL of DMSO. This was also dried down in a speedvac but only until it was in an almost dry tacky state. 10 μL of a $NaHCO_3$/NaOH buffer at pH 9 was added. The entire mixture was then dissolved in 500 μL of methanol and put in a small agate mortar. The mortar was placed under low vacuum for at least 5 h to evaporate the methanol. The 10 μL of a $NaHCO_3$/NaOH buffer helped to change the pH as the methanol evaporated ionizing the DOX-PCB to assist in the formation of the Captisol® complex.

After the methanol was evaporated from the mortar, 80 mg of Captisol® brand cyclodextrin dry powder was added and mechanically ground with the dried DOX-PCB with the small pestle until a fine purple colored powder was formed. 200 μL of sterile saline was added and then solution bath sonicated for 10 min. The maximum concentration achieved of the DOX-PCB in the Captisol® solution was 2 mM. The samples were centrifuged at 17 500 ***g*** for 5 min to eliminate any precipitated DOX-PCB. The concentration of DOX-PCB in the supernatant was then measured using absorbance on a NanoDrop ND-1000 spectrophotometer (Thermo Scientific, Wilmington, DE, USA).

DOX-PCB blood circulation half-life and urine elimination. Two female nude mice were injected with 200 μL of the DOX-PCB/Captisol® solution. Blood samples were collected at 5, 15, 30, 60 min and at 24 h. The blood was centrifuged and 15 μL of serum was collected. Urine was collected when naturally possible from the mouse out to 24 h.

Serum extraction method. 30 μL of acetonitrile (ACN) was added to the collected 15 μL blood serum samples from each time point. The samples were bath sonicated for 10 min. The sample was centrifuged at 17 500 ***g*** for 10 min and the supernatant collected. 30 μL of the supernatant was used for LC/mass analysis.

Urine extraction method. ACN was added to the urine sample (1:1) (vol:vol). The sample was then bath sonicated for 10 min. The sample was centrifuged at 17 500 ***g*** for 10 min. The supernatant was taken and dried in a speedvac. The precipitant was redissolved in 50 μL of ACN and sonicated. The sample was centrifuged again and the supernatant removed for analysis.

DOX-PCB activation in vivo. The experimental design for the *in vivo* activation is shown in Fig. 3. The 200 μL of DOX-PCB/Captisol® was injected slowly into the tail vein of two mice. The mice were anesthetized with 120 μL of ketamine 4 min later which was enough to keep the mouse anesthetized for the 30 min duration of the 365 nm light administration. Ten minutes after the DOX-PCB injection the 365 nm LED was inserted into the middle of the tumor and turned to full power delivering 240 $\mu W\ cm^{-2}$. Only the tumors on the right side of the mice were exposed. The 365 nm light was administered for a total of 30 min. Blood

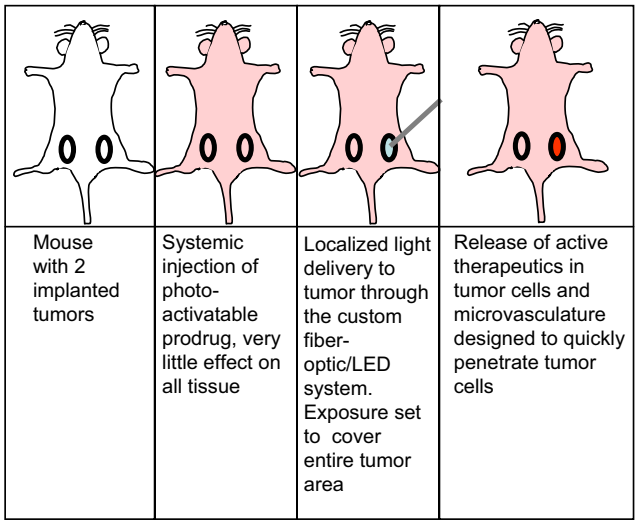

Figure 3. Schematic of photoactivatable prodrug delivery scheme and *in vivo* experimental setup.

was drawn right after the 365 nm light administration (40 min after injection) to obtain the circulating concentration. The mice were then sacrificed and the tumors and other internal organs collected for analysis.

DOX in vivo control. A control mouse was injected with a 2mM dose of DOX dissolved in saline with 80 mg of Captisol® to compare with DOX-PCB. The DOX mouse was treated the same as the DOX-PCB mice being given 120 μL of ketamine 4 min after tail vein injection. However, no 365 nm light was administered to the mouse. Blood was drawn at 30 min after injection to obtain the circulating concentration. The mouse was then sacrificed and the tumors and other internal organs collected for analysis. The tumor extraction from the DOX control mouse (data not shown) showed that DOX was present in the tumor when injected systemically confirming that this xenograft tumor model allowed drug accumulation within the tumor.

Tissue extraction protocol and LC-MS\MS method. Both the tumor tissue extraction protocol and the LC-MS\MS method used here to quantify the DOX and DOX-PCB content are fully detailed in the literature (36). These procedures were chosen because they were shown to have a detection limit of 7.8 pg for DOX from tumor tissue extraction samples. Achieving this low limit of detection was impart due to salt precipitations of the DNA to denature the double helix and release intercalated DOX with subsequent precipitation of the salt for LC-MS\MS compatibility. The high degree of DOX sensitivity was necessary due to the poorly vascularized nature of the A549 tumors where it was expected that small amounts of drug would accumulate.

RESULTS

Ex vivo 365 nm light penetration of tumor tissue

As discussed in the introduction, the photocleavable group of DOX-PCB was activated by 365 nm light which has minimal absorption by protein and DNA, but is highly adsorbed by melanin resulting in low skin penetration. Such characteristics enable 365 nm light penetration into soft tissues once delivered across the skin. The attenuation spectra for the tumor tissue was measured on a NanoDrop 1000 Spectrophotometer using a 4.9 mg tissue sample and is shown in Fig. 4A. The attenuation is 0.38 at 365 nm over a 0.2 mm path length. Not all of this attenuation is due to absorption. The 365 nm light is highly scattered in tissue (37) which helps to create a uniform coverage of the tumor area and contributes to the attenuation value. To establish effective 365 nm exposure through tumor tissue, including the tumor periphery, *ex vivo* tumor tissue samples were studied. The *ex vivo* tumors were exposed from the center and the resulting intensity of the light that penetrated through the surface of the tumor tissue was measured at different angles.

The intensity of the light coming from just the 365 nm LED/fiber-optic itself, without tumor tissue, was measured at 240 μW from 10 mm directly in front of the fiber-optic end. The 365 nm light was undetectable from 10 mm above the fiber-optic end and 10 mm from directly behind.

The same power settings were maintained and the fiber optic was inserted into the middle of a tumor sample. The 365 nm light was heavily scattered in the tissue causing it to exit the tumor tissue at all angles. A visual demonstration of the experiment is shown in Fig. 4B. The 365 nm light exiting the tumor surface is shown by autofluorescence on a piece of paper held behind the tumor. The measured intensity of the 365 nm light was 2 μW cm^{-2} from 10 mm directly in front, 2.9 μW cm^{-2} from 10 mm directly above and 1.4 μW cm^{-2} from 10 mm directly behind the tumor sample. The measured intensity above

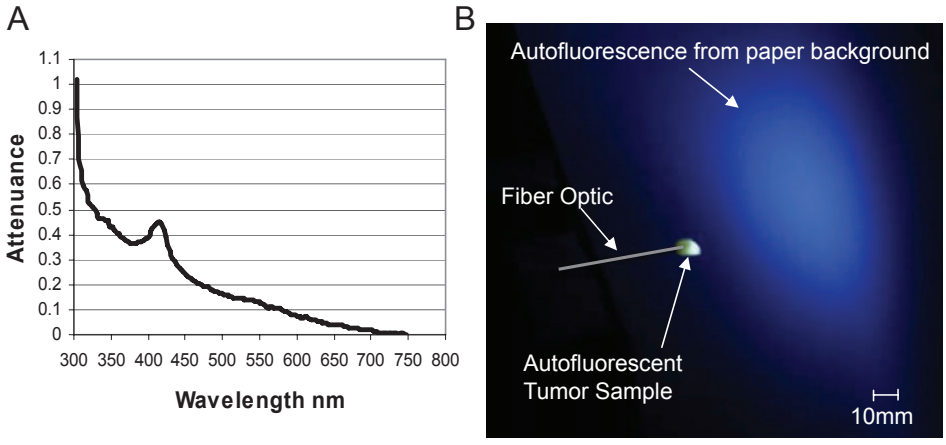

Figure 4. 365 nm light scattering and penetration through an excised tumor sample. (A) Attenuation spectra for the tumor tissue over a 0.2 mm path length. Attenuation is 0.38 at 365 nm which is contributed to by scattering as well as absorption. (B) The fiber optic is inserted into the center of a 9 × 6 × 5 mm tumor sample. The tumor glows light blue from 365 nm light-induced autofluorescence. A piece of white paper is placed behind the tumor and glows blue from the autofluorescence caused by the 365 nm light that exits the tumor sample.

the tumor was higher than directly in front due to the asymmetry of tissue distribution around the end of the fiber optic. When integrated over the surface of a 15 mm radius sphere the total amount of 365 nm light exiting the tumor is estimated to be 59.3 μW. Using uncaging rates already measured for DOX-PCB at 0.0031% μW^{-1} min^{-1} (19) the 59.3 μW would be sufficient intensity to uncage DOX-PCB at rate of 0.19%/min at the periphery of the 9 mm long tumor. After the 30 min exposure an estimated 5.7% of the DOX-PCB would be converted into DOX at the tumor periphery. The intensity of 365 nm light can be increased four times by directly inserting the LED into the tumor tissue, due to loss in the LED fiber-optic coupling. Directly inserting the LED's will be explored in future experiments. This shows that the 365 nm light has significant penetration through the tumor tissue to activate DOX-PCB.

The antitumor effect of just the 365 nm light itself is expected to be minimal based on observations of *in vitro* cancer cell viability (19). A549 human lung cancer cells were exposed to 1.8 mW cm^{-2} of 330–380 nm band pass filtered light from a mercury arc lamp with no observed change in viability out to 20 min of exposure.

DOX-PCB activation in *ex vivo* tumor tissue

The results of the *ex vivo* tumor exposure experiment are shown in Fig. 5. Figure 5A shows the tissue extraction LC/MS/MS trace for a tumor sample spiked with DOX, epirubicin (EPI) as an internal standard and DOX-PCB. Epirubicin is an isomeric form of DOX and can be separated from DOX on HPLC. Figure 5Ai shows the LC/MS/MS trace from a tumor spiked with DOX and EPI. Figure 5Aii shows the two DOX-PCB isomer peaks. Figure 5B shows the LC/MS/MS trace for the tumor sample spiked with just DOX-PCB and EPI. Trace 4Bi shows the presence of only EPI and trace 4Bii shows the presence of DOX-PCB. Figure 5C shows the trace for the tumor sample spiked with just DOX-PCB and EPI with subsequent exposure to 30 min of 365 nm light. As can be observed in trace 4Ci, the EPI peak is present along with a restored DOX peak. Moreover, the DOX-PCB peaks (trace 4Cii) have been dramatically reduced in magnitude. The disappearance of the DOX-PCB peak with the appearance of the DOX peak demonstrates that DOX-PCB can be converted into actual DOX within tissue using the 365 nm light.

In vivo activation of DOX-PCB in tumor tissue

After it was shown successfully that active DOX was formed upon local exposure of DOX-PCB in cell lines (19) and in *ex vivo* tumor tissue samples, a set of experiments were conducted to determine the *in vivo* accumulation of DOX-PCB in tumor tissue and the photocleavage of that DOX-PCB to active DOX. The steps in achieving this were to first solubilize DOX-PCB using Captisol® cyclodextrin to achieve high concentrations in saline for injection. The circulation half-life of the solubilized DOX-PCB was measured as well as urine content to look for elimination. The circulation half-life was used to determine the best time to start 365 nm exposure of the tumor tissue to prevent significant activation of DOX-PCB in the tumor vasculature. Reducing free DOX production in the vasculature should reduce the possibility of free DOX being swept into systemic circulation. The tumor samples were then analyzed for DOX-PCB and

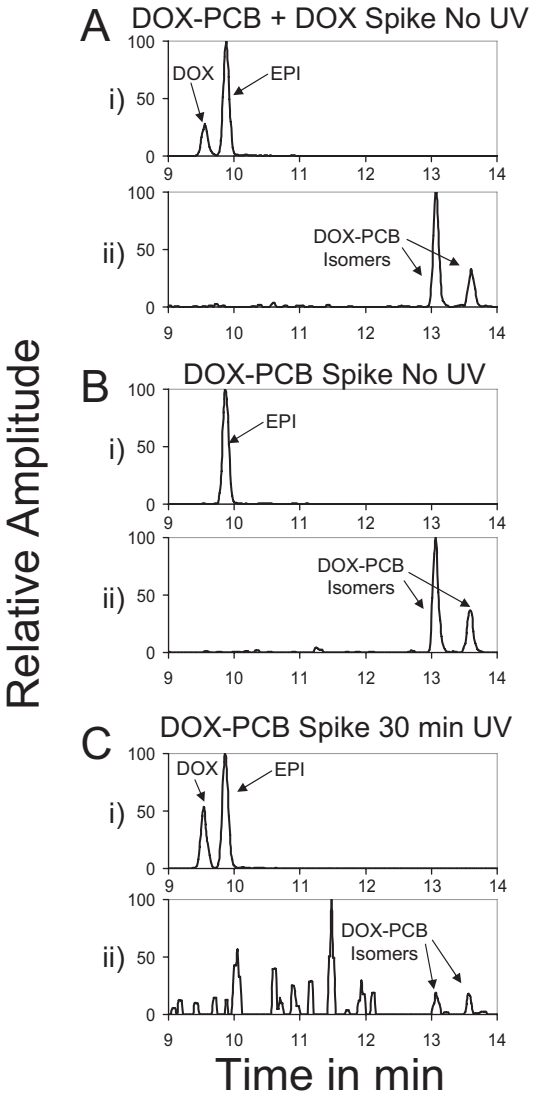

Figure 5. LC/MS/MS traces of an *ex vivo* tumor tissue extraction. The tumor tissue samples were spiked with: (A) DOX and the internal standard EPI (i), DOX-PCB (ii); (B) EPI (i), DOX-PCB (ii); (C) EPI and DOX-PCB and then exposed to 30 min of 365 nm light from the LED system. As can be seen the DOX peak is restored (i) whereas the DOX-PCB isomer peaks are greatly reduced in intensity (ii). Additional peaks appear along with the DOX-PCB peaks because the DOX-PCB concentration has been reduced to the point where it is no longer the dominate compound in the sample.

DOX content. EPI was spiked into these tumor samples during the extraction process to serve as an internal standard.

DOX-PCB solubilization with Captisol® cyclodextrin

The solubilization of DOX-PCB with Captisol® cyclodextrin was successful and resulted in the desired concentration of 1.2 mg of DOX-PCB in 200 μL of saline. The three dimensional structure of the β-cyclodextrin molecule (38) has a hydrophobic internal barrel. Captisol® is a slightly modified version of β-cyclodextrin where a sulfobutylether is used to separate a sodium sulfonate salt from the hydrophobic cavity to improve water solubility. The structure of DOX interacting with the hydrophobic barrel through the conjugated ring structure has been proposed (38) and should

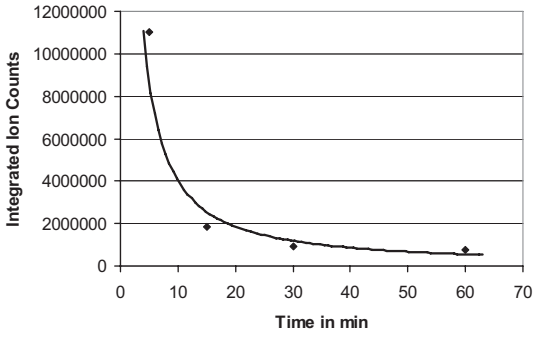

Figure 6. The serum concentration of DOX-PCB as a function of time as measured by LC/MS. No DOX was detected at any time point.

be similar to how DOX-PCB interacts with the cyclodextrin. Interaction with the hydrophobic barrel of the cyclodextrin prevents interaction between the hydrophobic conjugated ring structure of DOX and the hydrophobic nitrophenyl compound avoiding aggregation in saline solution.

DOX-PCB circulation half-life and urine concentration

DOX-PCB circulation *in vivo* was studied by analyzing serum samples collected at different time points from mice injected with the DOX-PCB/Captisol® complex. DOX-PCB was found to have an alpha phase circulation half-life of 10 min (Fig. 6), which is comparable to that of DOX at around 20 min (39). No DOX was found in the blood at any time point.

No DOX-PCB or DOX was found in the urine at any of the collected time points out to 24 h (data not shown). The absence of DOX in the serum and urine indicated that there is no metabolic or self-conversion of DOX-PCB to DOX. This is consistent with earlier findings that DOX-PCB was resistant to metabolic activation when incubated with human liver microsomes (19). This establishes exposure to 365 nm light as the major mode of activation.

DOX-PCB activation *in vivo*

Two tumors were collected from each DOX-PCB injected mouse. Only one of the two tumors was exposed to the 365 nm light with the other serving as a control. The tumors collected from the mice were sectioned into six pieces as shown in Fig. 7A,B. The tumors were not spherical but rather oblong in shape as shown schematically edge on in Fig. 7A. The line down the center shows where the tumor was cut in half. The two halves were subsequently cut into six pieces as shown in Fig. 7B. The mass of the different pieces from both Mouse 1 and 2 is shown in Table 1. This dissection scheme was designed to fulfill two requirements. The first was to obtain tissue samples that had individual masses between 30 and 60 mg. It was found that this mass range worked best for the extraction protocol. Tissue samples larger than 60 mg showed incomplete freeze fracturing reducing the extraction efficiency. Tissue samples above 30 mg ensured that sufficient DOX would be present to yield a clear signal. The second requirement was to understand the DOX distribution throughout the entire tumor. The LED fiber-optic needle was inserted into the center of the tumor so the tumor was first dissected down the center through where the needle end had been. The two end sections 1 and 4 were combined to meet the tissue mass requirement and to represent one extreme end of the tumor. Sections 3 and 6 were likewise combined to represent the other extreme end of the tumor. Sections 2 and 5 met the mass requirements individually and represented two halves of the central portion of the tumor closest to the needle insertion site. The tumors from Mouse 1 were bigger and more vascularized than the tumors from Mouse 2.

DOX-PCB was found in all sections of the tumor tissue in both the exposed and unexposed tumors for both mouse 1 and 2. As an example, the LC/MS/MS data from the Mouse 1 tumors are shown in Fig. 7C–F and Fig. 8C–F. For both Mouse 1 and 2, DOX appeared in all four sections in roughly equal amounts of the 365 nm light-exposed tumor as shown in Fig. 7C–F. A trace amount of DOX was found in two sections of the unexposed tumor as shown in Fig. 8C and f covering the left side of the tumor in Mouse 1. Mouse 2 showed a trace amount of DOX in only one side of the tumor as well.

To summarize the data shown in Fig. 7, each of the four graphs were adjusted to account for small elution time differences from run to run and then added together and normalized as shown in Fig. 9A. This gives the relative amplitude of DOX to the EPI internal standard for the entire 365 nm light-exposed tumor. The same was done for the four graphs in Fig. 8 and the summed results are shown in Fig. 9B. The intensity of the EPI internal standard is the same in Fig. 9A,B allowing both to be directly compared. The 365 nm light-exposed tumor had a higher amount of DOX than the unexposed tumor due to the conversion of DOX-PCB into DOX. This trend was the same for the second mouse as well.

No DOX was found in the serum of the mouse after the 30 min of 365 nm light exposure in the tumor as shown in Fig. 10.

Preferential DOX accumulation in the 365 nm light-exposed tumor

The same amount of EPI internal standard was spiked into each extraction sample to evaluate and quantitize DOX formation within the tumors. This allowed a ratio to be calculated between the area under the curve of the LC/MS/MS traces for DOX and EPI. This ratio allowed for direct comparisons to be made between different samples to estimate relative DOX amounts in each. This allowed for direct comparison between the 365 nm light-exposed and unexposed tumors as well as between the two mice. When the mass of the entire tumor was accounted for, there was six times more DOX/gram of tissue in the tumor

Table 1. Mass in grams of the different tumor sections for both the 365 nm light-exposed and unexposed tumors.

	Mouse 1		Mouse 2	
Tumor section	No 365 nm light	30 min 365 nm light	No 365 nm light	30 min 365 nm light
1	0.0255	0.0496	0.0247	0.0163
2	0.0405	0.0825	0.0237	0.0354
3	0.0267	0.0426	0.0254	0.0101
4	0.0334	0.0382	0.0262	0.0125
5	0.0534	0.0833	0.0286	0.0104
6	0.0258	0.0547	0.0131	0.0217
Total	0.2053	0.3509	0.1417	0.1064

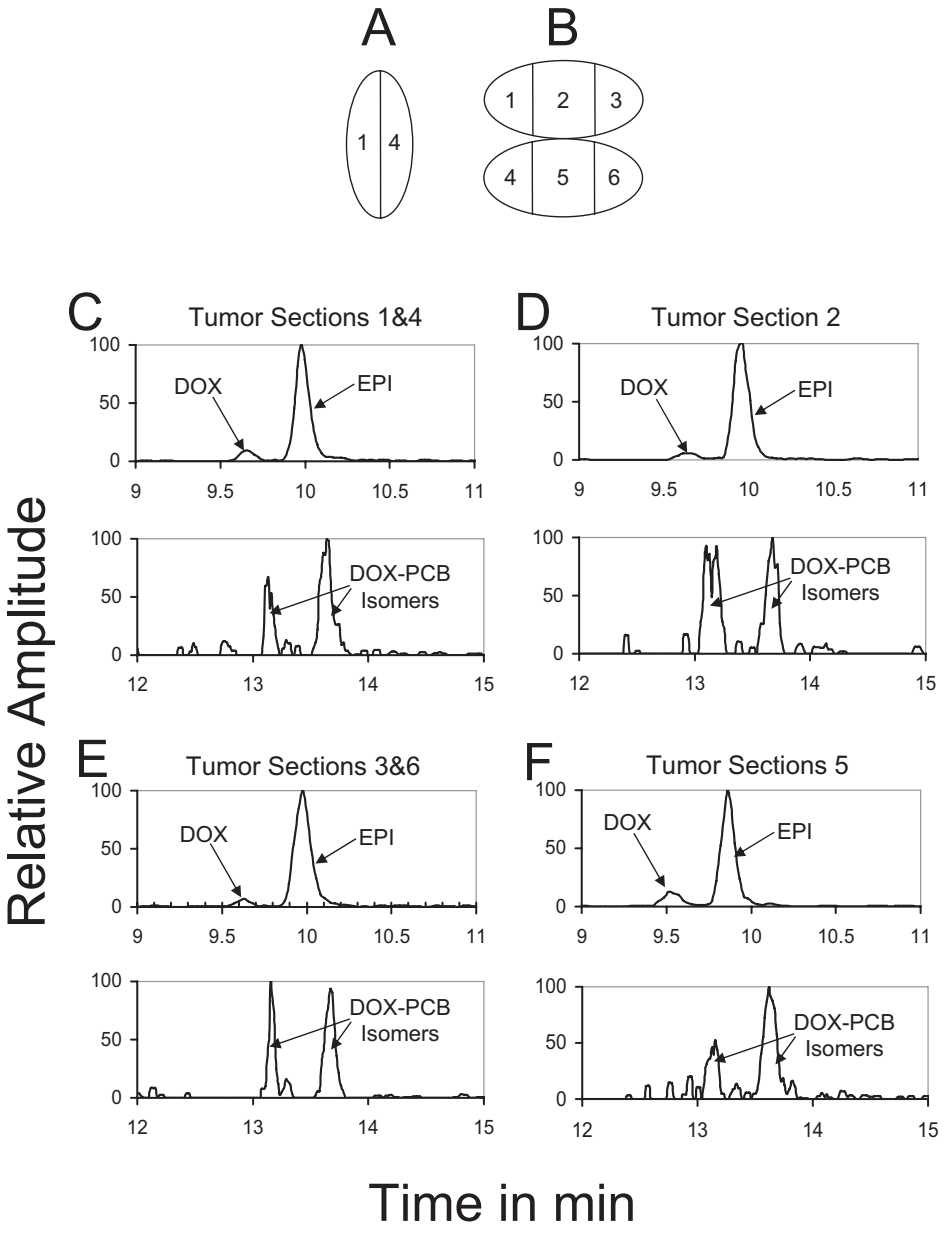

Figure 7. Tumor sectioning procedure and the LC/MS/MS data showing the presence of DOX-PCB, EPI and DOX in the *in vivo* tumor tissue exposed to 30 min of 365 nm light for Mouse 1. (A) Edge-on view of the tumor in schematic representation showing how the tumor was sectioned in half. (B) Open view of the halved tumor showing the numbered sections. (C) LC/MS/MS traces of the tumor tissue extraction for combined pieces 1 and 4 showing both DOX and DOX-PCB presence. (D) LC/MS/MS traces for piece 2 showing both DOX and DOX-PCB presence. (E) LC/MS/MS traces of the tumor tissue extraction for combined pieces 3 and 6 showing both DOX and DOX-PCB presence. (F) LC/MS/MS traces for piece 5 showing both DOX and DOX-PCB presence.

exposed to 365 nm light than the unexposed control tumor. Mouse 1 had 6.1 times more DOX in the 365 nm light-exposed tumor. In this case, the 365 nm light-exposed tumor was bigger than the unexposed tumor and had better vascularization of the outer margins. Mouse 2 had a ratio of 6.0 times more DOX in the 365 nm light-exposed tumor. In this case the 365 nm light-exposed tumor was smaller and was less vascularized than the control tumor. There appears to be little migration effect of the DOX into systemic circulation, even when the tumors were more vascularized.

DISCUSSION

In this work we have demonstrated the activation of the new DOX-PCB photocleavable prodrug inside of both *ex vivo* and *in vivo* tumor tissue. The *ex vivo* tissue penetration of the 365 nm light was sufficient through a 9 mm tumor sample to uncage DOX-PCB at an estimated rate of 0.19% per min at the periphery of the tumor. This rate can be increased at least four times by using more powerful LED light sources and directly inserting the LED itself into the tumor tissue. These results demonstrate

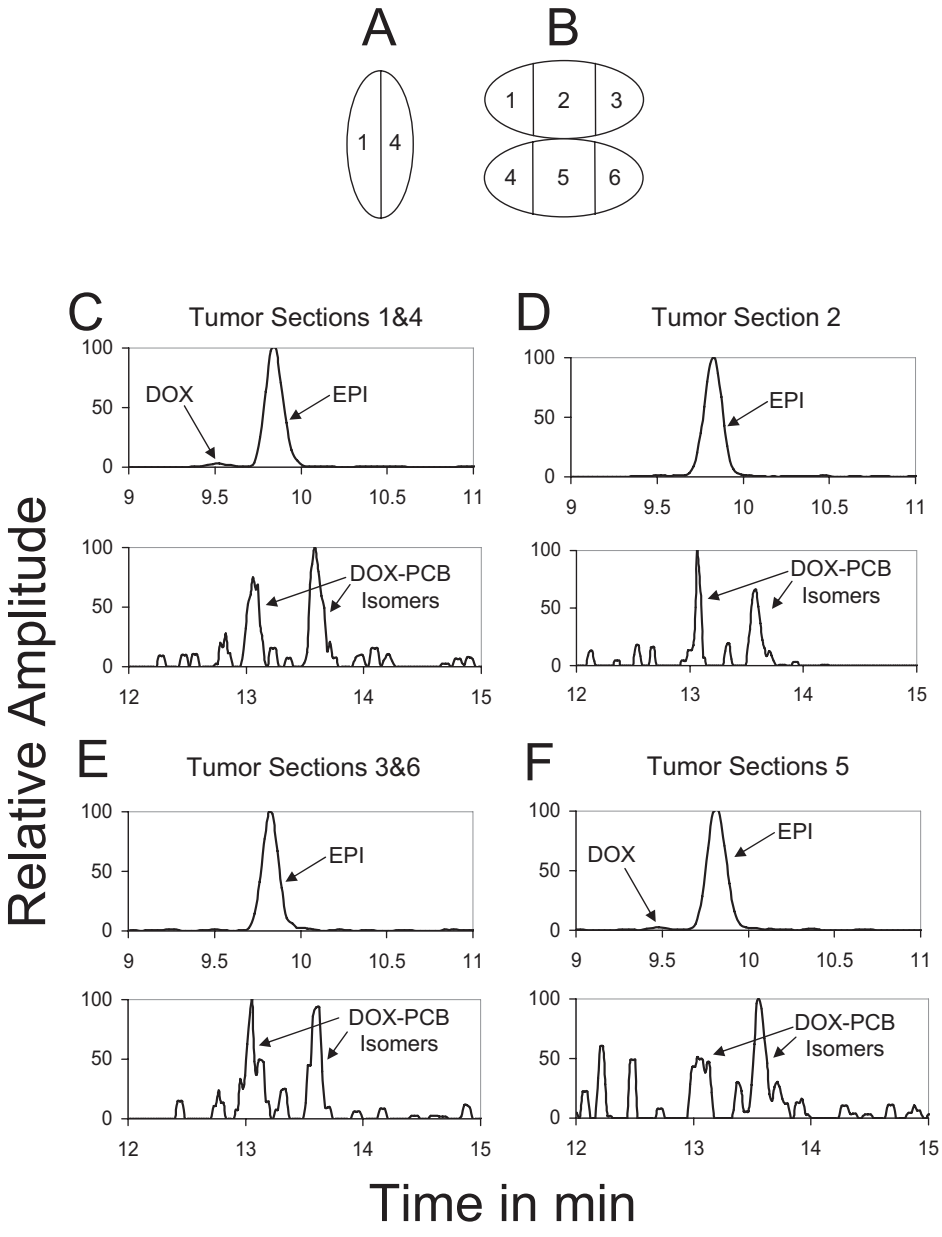

Figure 8. Tumor sectioning procedure and the LC/MS/MS data showing the presence of DOX-PCB, EPI and a trace amount of DOX in the *in vivo* tumor tissue not exposed to 365 nm light for Mouse 1. (A) Edge-on view of the tumor in schematic representation showing how the tumor was sectioned in half. (B) Open view of the halved tumor showing the numbered sections. (C) LC/MS/MS traces of the tumor tissue extraction for combined pieces 1 and 4 showing DOX-PCB presence and a trace amount of DOX. (D) LC/MS/MS traces for piece 2 showing only DOX-PCB presence. (E) LC/MS/MS traces of the tumor tissue extraction for combined pieces 3 and 6 showing only DOX-PCB presence. (F) LC/MS/MS traces for piece 5 showing DOX-PCB presence and a trace amount of DOX.

that tissue does not inhibit DOX-PCB activation and that the 365 nm light has significant penetration through several millimeters of tissue.

The 10 min α phase circulation half-life of DOX-PCB was comparable with the 20 min half-life of DOX showing that DOX-PCB was not immediately removed by the liver. The lack of DOX in the serum or the urine showed that DOX-PCB was resistant to normal metabolic processes. This also indicates that any DOX produced in the body would most likely be a result of the light activation pathway.

The preliminary *in vivo* activation data show that DOX-PCB made it to the tumor tissue where it was converted into DOX in measurable quantities. This is significant because the tumor tissue was poorly vascularized reducing the efficiency of any compound to accumulate. The absence of DOX in the serum showed that DOX generated by the 365 nm light did not get immediately swept into circulation and was able to penetrate into the local tumor tissue, or was released within the cells themselves. This makes it unlikely that a significant systemic exposure would occur from DOX activated within the tumor.

The small amount of DOX found on one side of the unexposed control tumor was surprising given that DOX-PCB was resistant to metabolic activation and no DOX was found in circulation. This means that the DOX was most likely formed by

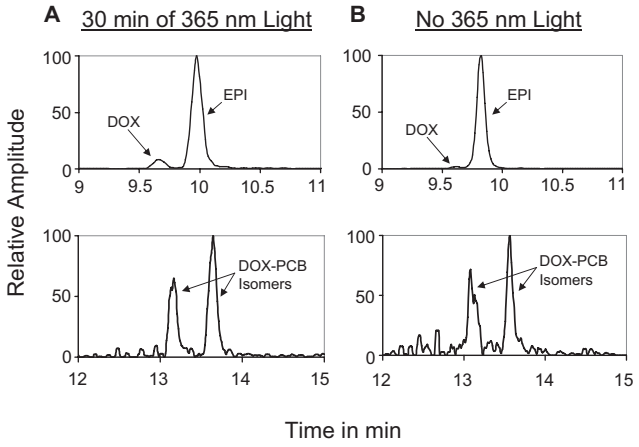

Figure 9. Summary of the data shown in Figs. 7 and 8. (A) The four individual tumor section graphs from Fig. 7 were adjusted for elution time differences and added together to give the total DOX content of the 365 nm light-exposed tumor. The intensity of the DOX peak is scaled by the EPI internal standard peak. (B) The four graphs in Fig. 8 were analyzed in the same manner to give the DOX content of the tumor not exposed to the 365 nm light scaled to the EPI internal standard. The EPI internal standard peaks have the same intensity in both frames A and B allowing the DOX content of the two tumors to be directly compared. More DOX was seen in the 365 nm light-exposed tumor.

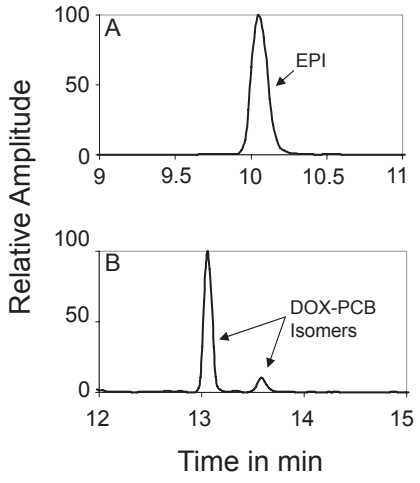

Figure 10. LC/MS/MS trace of the serum extraction preformed on the serum collected after 30 min of light exposure in Mouse 1. No DOX was found indicating that the activated DOX was not immediately swept into circulation in measurable quantities, but primarily stayed within the tissue where it was activated.

exposure to 365 nm light that leaked out of the exposed tumor. The nude mice used were albino and lacked melanin in the skin which allowed the 365 nm light to leave the exposed tumor and expose the facing half of the control tumor just 10 mm away. Without this leaked 365 nm light, the ratio of activated DOX between the exposed and unexposed tumors would have been higher than the six times shown in this work.

In the human application, sensitive organs such as the heart can be considerably further away than a few centimeters from the tumor making 365 nm light exposure negligible. Achieving this level of tumor localization can be a challenge for the highly penetrating red or near IR light wavelengths used to activate photodynamic therapy compounds (PDT) (40). These PDT compounds produce free radicals creating a cytotoxic amount of indiscriminate cellular damage to both tumor and healthy tissue (41). The therapeutic mechanism of DOX on the other hand has a level of tumor specificity. DOX is well known to preferentially accumulate in the DNA causing damage and preventing cellular replication (19) and thereby having the greatest effect on rapidly dividing cells (42,43). The advancing tumor margins are in direct contact with healthy tissue and are a major target of chemotherapy treatment (44). It is desirable to have the light exposure extend just one or two centimeters beyond the tumor margin to make sure these regions get a significant dose. DOX-PCB activation in the healthy tissue of these margins would have a much lower toxic effect than the activation of PDT compounds (41). The efficiency of the photoactivation needs to be considered as well. DOX-PCB activation is more efficient at wavelengths below 365 nm, but tissue penetration at these wavelengths is negligible, preventing uncontrolled release from occurring. The efficiency of 365 nm light activation can be compensated for by simply increasing the exposure time in the tumor region.

The photoactivation of prodrug inside the tumor cells and tumor microvasculature is different from an intratumoral injection of pure DOX. When injecting drug directly into the tumor tissue most of the injectant is forced into the interstitial space between tumor cells and is quickly swept into the lymph system (45). This limits the distance that the drug can diffuse away from the needle. Although the center of the tumor might get a therapeutic dose, the limited diffusion makes it difficult to achieve a therapeutic concentration of drug at the advancing tumor margins where it is needed most (46). The prodrug, however, is delivered to the tumor through the vasculature and so reaches every part of the tumor that has an active blood supply, including the well-vascularized tumor margins. The tumor tissue scatters the 365 nm light delivered to the tumor center to achieve prodrug activation throughout the whole region including the margins. As the activated DOX was quickly taken up by nearby cells it did not have a chance to enter systemic circulation, keeping the drug in the tumor tissue.

Another challenge with intratumoral injection is that the tumor tissue tends to be denser than healthy tissue, like muscle, requiring a higher injection pressure. During intratumoral injection the drug can simply follow the path of least resistance and reflux straight back up the needle track. This spreads the highly concentrated drug to healthy tissues along the way causing necrosis and pain (47,48). As the light activation method does not require an injection pressure, there is no driving force to send the activated drug up the fiber-optic track. During these experiments no reflux was observed from the fiber-optic insertion site of the tumor.

The pharmacokinetics, lack of metabolic activation and localized *in vivo* light activation of DOX-PCB as described here demonstrate the desirable qualities of this compound. The 200 times reduction in cytotoxicity of DOX-PCB should allow larger doses to be administered than possible with pure DOX. This increases the amount that could reach even poorly vascularized tumors. The localized release of fully toxic DOX from DOX-PCB can help create significant tumor response and should reduce side effects.

CONCLUSIONS

The DOX-PCB prodrug, solubilized with Captisol® cyclodextrin, was found to have a circulation half-life of 10 min which was sufficient time to reach even poorly vascularized tumor tissue. The 365 nm light, administered with the LED/fiber-optic system, was shown to penetrate the tumor tissue to sufficiently release measurable amounts of pure DOX from DOX-PCB at the tumor periphery and within the tumor tissue. Tumor tissue exposed to the light had six times more DOX than tumor tissue from the same animal that did not have direct light exposure, demonstrating preferential tumor tissue retention. No DOX was found in the serum sample collected after the 30 min light exposure indicating that activated DOX was not immediately swept into systemic circulation, but rather stayed within the tissue where it was activated. This demonstrates a proof of concept for the approach of using photoactivation as a trigger to achieve localized prodrug activation in deep tumors.

Acknowledgements—The authors are grateful for the support of Howard Cottam in the collection and interpretation of the data. The authors also wish to thank Ambergen Inc, for clarification of the structural details of the PCB diastereoisomers. The study was supported by the National Cancer Institute grant # 5 U54 CA119335.

REFERENCES

1. Cvetkoviand, R. S. and L. J. Scott (2005) Dexrazoxane: A review of its use for cardio protection during anthracycline chemotherapy. *Drugs* **65**, 1005–1024.
2. Pawan, N. I. and K. Singal (1998) Doxorubicin-induced cardiomyopathy. *N. Engl. J. Med.* **339**, 900–905.
3. Metzger, M. L., J. S., Dome (2005) Current therapy for Wilms' tumor. *Oncologist* **10**, 815–826.
4. D'Angio, G. J. (2003) Pre- or post-operative treatment for Wilms tumor? Who, What, When, Where, How, Why—and Which. *Med. Pediatr. Oncol.* **41**, 545–549.
5. Shapiroand, C. and A. Recht (2001) Side effects of adjuvant treatment of breast cancer. *N. Engl. J. Med.* **344**, 1997–2008.
6. Demetri, G. D., A. L. Cesne, S. P. Chawla, T. Brodowicz, R. G. Maki, B. A. Bach, D. P. Smethurst, S. Bray, Y.-j. Hei and J.-Y. Blay (2012) First-line treatment of metastatic or locally advanced unresectable soft tissue sarcomas with conatumumab in combination with doxorubicin or doxorubicin alone: A phase I/II open-label and double-blind study. *Eur. J. Cancer*. Online.
7. Olson R. D., P. S. Mushlin, (1990) Doxorubicin cardiotoxicity: Analysis of prevailing hypotheses. *FASEB J.* **4**, 3076–3086.
8. Giorgio Minotti, P. M., E. Salvatorelli, G. Cairo and L. Gianni (2004). Anthracyclines: Molecular advances and pharmacologic developments in antitumor activity and cardiotoxicity. *Pharmacol. Rev.* **56**, 185–229.
9. Ewer, M. S., N. Jaffe, H. Ried, H. A. Zietz and R. S. Benjamin (1998). Doxorubicin cardiotoxicity in children: Comparison of a consecutive divided daily dose administration schedule with single dose (rapid) infusion administration. *Med. Pediatr. Oncol.* **31**, 512–515.
10. Mertens, A. C., Y. Yasui, J. P. Neglia, J. D. Potter, M. E. N. Jr, K. Ruccione, W. A. Smithson and L. L. Robison (2001). Late mortality experience in five-year survivors of childhood and adolescent cancer: The childhood cancer survivor study. *J. Clin. Oncol.* **19**, 3163–3172.
11. Gabizon, A. A. (2001) Pegylated liposomal doxorubicin: Metamorphosis of an old drug into a new form of chemotherapy. *Cancer Invest.* **19**, 424–436.
12. O'Brien, M. E. R., N. Wigler, M. Inbar, R. Rosso, E. Grischke, A. Santoro, R. Catane, D. G. Kieback, P. Tomczak, S. P. Ackland, F. Orlandi, L. Mellars, L. Alland and C. Tendler (2004). Reduced cardiotoxicity and comparable efficacy in a phase III trial of pegylated liposomal doxorubicin HCl (CAELYX™/DoxiR) versus conventional doxorubicin for first-line treatment of metastatic breast cancer. *Ann. Oncol.* **15**, 440–449.
13. Cheong, I., X. Huang, C. Bettegowda, L. A., Jr Diaz, K. W. Kinzler, S. Zhou and B. Vogelstein (2006). A bacterial protein enhances the release and efficacy of liposomal cancer drugs. *Science* **314**, 1308–1311.
14. Moghimi, S. M., A. C. Hunter and J. C. Murray (2001). Long-circulating and target-specific nanoparticles: Theory to practice. *Pharmacol. Rev.* **53**, 283–318.
15. Wood, B. J., R. T. Poon, J. K. Locklin, M. R. Dreher, M. Eugeni, G. Seidel, S. Dromi, Z. Neeman, M. Kolf, C. D. V. Black, R. Prabhakar and S. K. Libutti (2012). Phase I study of heat-deployed liposomal doxorubicin during radiofrequency ablation for hepatic malignancies. *J. Vasc. Interv. Radiol.* **23**, 248–255.
16. Wang, S., S. P. Mahesh, J. Liu, C. Geist and V. Zderic (2012). Focused ultrasound facilitated thermo-chemotherapy for targeted retinoblastoma treatment: A modeling study. *Exp. Eye Res.* **100**, 17–25.
17. Niand, T. and Baudisch, P. (2009) Disappearing mobile devices, Proceedings of the 22nd annual ACM symposium on User interface software and technology, Association for Computing Machinery, Victoria, British Columbia, Canada, pp. 101–110.
18. Amit, B., U. Zehavi and A. Patchornik (1974). Photosensitive protecting groups of amino sugars and their use in glycoside synthesis. 2-nitrobenzyloxycarbonylamino and 6-nitroveratryloxycarbonylamino derivatives. *J. Org. Chem.* **39**, 192–196.
19. Ibsen, S., E. Zahavy, W. Wrasdilo, M. Berns, M. Chan and S. Esener (2010). A novel doxorubicin prodrug with controllable photolysis activation for cancer chemotherapy. *Pharm. Res.* **27**, 1848–1860.
20. Miwa, M., M. Ura, M. Nishida, N. Sawada, T. Ishikawa, K. Mori, N. Shimma, I. Umeda and H. Ishitsuka (1998). Design of a novel oral fluoropyrimidine carbamate, capecitabine, which generates 5-fluorouracil selectively in tumours by enzymes concentrated in human liver and cancer tissue. *Eur. J. Cancer* **34**, 1274–1281.
21. Denny, W. A. (2001). Prodrug strategies in cancer therapy. *Eur. J. Med. Chem.* **36**, 577–595.
22. Denny, W. A. (2004). Tumor-activated prodrugs—a new approach to cancer therapy. *Cancer Invest.* **22**, 604–619.
23. Lutz, M. N., F. Tietze, T. Mollers, R. Fischer, K.-H. Glusenkamp, M. F. Rajewsky and E. Jahde (1989). Proton-mediated liberation of aldophosphamide from a nontoxic prodrug: A strategy for tumor-selective activation of cytocidal drugs. *Cancer Res.* **49**, 4179–4184.
24. Martin Brown, W. R. W. J. (2004). Exploiting tumor hypoxia in cancer treatment. *Nat. Rev. Cancer* **4**, 437–447.
25. Breistol, H. R. H. K., D. P. Berger, S. P. Langdon, H. H. Fiebig and O. Fodstad (1998). The antitumour activity of the prodrug N-l-leucyl-doxorubicin and its parent compound doxorubicin in human tumour xenografts. *Eur. J. Cancer* **34**, 1602–1606.
26. Gopin, A., S. Ebner, B. Attali and D. Shabat (2006). Enzymatic activation of second-generation dendritic prodrugs: Conjugation of self-immolative dendrimers with PEG via click chemistry. *Bioconjugate Chem.* **17**, 1432–1440.
27. Shamis, M., H. N. Lode and D. Shabat (2004). Bioactivation of self-immolative dendritic prodrugs by catalytic antibody 38C2. *JACS* **126**, 1726–1731.
28. Barbara, W. A. W., M. Mueller and R. A. Reisfeldt (1990). Antibody conjugates with morpholinodoxorubicin and acid-cleavable linkers. *Bioconjugate Chem.* **1**, 325–330.
29. Park, J., K. Hong, D. Kirpotin, G. Colbern, R. Shalaby, J. Baselga, Y. Shao, U. Nielsen, J. Marks, D. Moore, D. Papahadjopoulos and C. Benz (2002). Anti-HER2 immunoliposomes: Enhanced efficacy attributable to targeted delivery. *Clin. Cancer Res.* **8**, 1172–1181.
30. Vaupel, P., F. Kallinowski and P. Okunieff (1989). Blood flow, oxygen and nutrient supply, and metabolic microenvironment of human tumors: A review. *Cancer Res.* **49**, 6449–6465.
31. Dominic, R. H. S., A. Scudiere, K. D. Paull, A. Monks, S. Tierney, T. H. Nofziger, M. J. Currens, D. Seniff and M. R. Boyd (2004). A distinct "side population" of cells with high drug efflux capacity in human tumor cells. *PNAS* **101**, 14228–14233.
32. Fradet, Y., N. Islam, L. Boucher, C. Parent-Vaugeois and M. Tardif. (1987). Polymorphic expression of a human superficial bladder tumor antigen defined by mouse monoclonal antibodies. *Proc. Natl. Acad. Sci. U S A* **00**, 84.
33. Fradet, Y., N. Islam, L. Boucher, C. Parent-Vaugeois and M. Tardif (1987). Polymorphic expression of a human superficial bladder

tumor antigen defined by mouse monoclonal antibodies. *Proc. Natl. Acad. Sci. U S A* **84**, 7227–7231.
34. Yuanlong Yang, E. J. C., J. A. Koutcher and R. R. Alfano (2001). UV reflectance spectroscopy probes DNA and protein changes in human breast tissues. *J. Clin. Laser Med. Surg.* **19**, 35–39.
35. Sutherland, J. and K. Griffin (1981). Absorption spectrum of DNA for wavelengths greater than 300 nm. *Radiat. Res.* **86**, 399–410.
36. Ibsen, S., Y. Su, J. Norton, E. Zahavy, T. Hayashi, S. Adams, W. Wrasidlo and S. Esener. (In submission). Development of a Mass Spectrometry and Tissue Extraction Method to Detect Small Amounts of Photoreleased Doxorubicin in Tumor Tissue. *J. Mass Spectromet*.
37. Staveren, H. J. V., C. J. M. Moes, J. V. Marie, S. A. Prahl and M. J. C. V. Gemert. (1991). Light scattering in Intralipid-1 0% in the wavelength range of 400-1 1 00 nm. *Appl. Opt.* **30**, 4507–4515.
38. Loftssonand, T. and M. E. Brewster (1996). Pharmaceutical applications of cyclodextrins. 1. Drug solubilization and stabilization. *J. Pharm. Sci.* **85**, 1017–1025.
39. Johansen, P. B. (1981). Doxorubicin pharmacokinetics after intravenous and intraperitoneal administration in the nude mouse. *Cancer Chemother. Pharmacol.* **5**, 267–270.
40. Dolmans, D. E. J. G. J., D. Fukumura and R. K. Jai (2003). Photodynamic therapy for cancer. *Nat. Rev. Cancer* **3**, 380–387.
41. Hendersonand, B. and T. Dougherty (1992). How does photodynamic therapy work? *Photochem. Photobiol.* **55**, 145–157.
42. Quigley, G. J., A. H.-J. Wang, G. Ughetto, G. V. D. Marel, J. H. V. Boom and A. Rich (1980). Molecular structure of an anticancer drug-DNA complex: Daunomycin plus d(CpGpTpApCpG). *Proc. Natl. Acad. Sci. U S A* **77**, 7204–7208.
43. Gewirtz, D. A. (1999). A critical evaluation of the mechanisms of action proposed for the antitumor effects of the anthracycline antibiotics adriamycin and daunorubici. *Biochem. Pharmacol.* **57**, 727–741.
44. Neoptolemos, J. P., D. D. Stocken, J. A. Dunn, J. Almond, H. G. Beger, P. Pederzoli, C. Bassi, C. Dervenis, L. Fernandez-Cruz, F. Lacaine, J. Buckels, M. Deakin, F. A. Adab, R. Sutton, C. Imrie, I. Ihse, T. Tihanyi, A. Olah, S. Pedrazzoli, D. Spooner, D. J. Kerr, H. Friess and M. W. Büchler (2001). Influence of resection margins on survival for patients with pancreatic cancer treated by adjuvant chemoradiation and/or chemotherapy in the ESPAC-1 randomized controlled trial. *Ann. Surg.* **234**, 758–768.
45. Roelcke, U., O. Hausmann, A. Merlo, J. Missimer, R. P. Maguire, P. Freitag, E. W. Radü, R. Weinreich, O. Gratzl and K. L. Leenders (2002). PET imaging drug distribution after intratumoral injection: The case for 124I-iododeoxyuridine in malignant gliomas. *J. Nucl. Med.* **43**, 1444–1451.
46. Currier, M. A., L. C. Adams, Y. Y. Mahller and T. P. Cripe (2005). Widespread intratumoral virus distribution with fractionated injection enables local control of large human rhabdomyosarcoma xenografts by oncolytic herpes simplex viruses. *Cancer Gene. Ther.* **12**, 407–416.
47. Fiandaca, M. S., J. R. Forsayeth, P. J. Dickinson and K. S. Bankiewicz (2008). Image-guided convection-enhanced delivery platform in the treatment of neurological diseases. *Neurotherapeutics* **5**, 123–127.
48. Lammers, T., P. Peschke, R. Kühnlein, V. Subr, K. Ulbrich, P. Huber, W. Hennink and G. Stormy (2006). Effect of intratumoral injection on the biodistribution and the therapeutic potential of HPMA copolymer-based drug delivery systems. *Neoplasia* **8**, 788–795.